FISEVIER

Contents lists available at ScienceDirect

Journal of Inorganic Biochemistry

journal homepage: www.elsevier.com/locate/jinorgbio



Heme pocket modulates protein conformation and diguanylate cyclase activity of a tetrameric globin coupled sensor

Jacob R. Potter^a, Shannon Rivera^{d,1}, Paul G. Young^{d,1}, Dayna C. Patterson^e, Kevin E. Namitz^{e,f}, Neela Yennawar^f, James R. Kincaid^{b,2,***}, Yilin Liu^{b,c,**}, Emily E. Weinert^{a,e,*}

ARTICLE INFO

Keywords: Heme Small angle X-ray scattering Resonance Raman Oxygen sensing Globin Dieuanylate cyclase

ABSTRACT

Bacteria use the second messenger cyclic dimeric guanosine monophosphate (c-di-GMP) to control biofilm formation and other key phenotypes in response to environmental signals. Changes in oxygen levels can alter c-di-GMP signaling through a family of proteins termed globin coupled sensors (GCS) that contain diguanylate cyclase domains. Previous studies have found that GCS diguanylate cyclase activity is controlled by ligand binding to the heme within the globin domain, with oxygen binding resulting in the greatest increase in catalytic activity. Herein, we present evidence that heme-edge residues control O_2 -dependent signaling in PccGCS, a GCS protein from Pectobacterium carotovorum, by modulating heme distortion. Using enzyme kinetics, resonance Raman spectroscopy, small angle X-ray scattering, and multi-wavelength analytical ultracentrifugation, we have developed an integrated model of the full-length PccGCS tetramer and have identified conformational changes associated with ligand binding, heme conformation, and cyclase activity. Taken together, these studies provide new insights into the mechanism by which O_2 binding modulates activity of diguanylate cyclase-containing GCS proteins.

1. Introduction

The ability to sense molecular oxygen (O_2) is important for bacterial survival due to its role in metabolism and regulating both bacterial behavior and host-microbe interactions [1–4]. Because of this, bacteria have evolved a widespread family of O_2 -sensing hemoproteins termed globin coupled sensors (GCS) [5–7], which are implicated in the regulation of a variety of O_2 -dependent phenotypes [7], such as motility [8–10], virulence [8,9,11], and biofilm formation [3,8,9]. Diguanylate cyclase-containing globin coupled sensor (DGC-GCS) proteins are of particular interest because diguanylate cyclases (DGCs) are responsible

for synthesis of cyclic di-GMP (c-di-GMP), a bacterial second messenger that regulates biofilm formation [8,10]. Despite important roles for these proteins in modulating biofilm formation and virulence [3,9,11], a molecular level mechanism by which the O_2 binding signal is communicated from the globin domain to the DGC output domain remains elusive.

A major impediment to a detailed mechanism is the lack of full-length structural information for GCS proteins, leading to uncertainty regarding which residues are necessary for signaling and the three-dimensional structure/interactions of these proteins. This has been particularly challenging for GCS proteins containing DGC domains, as

^a Department of Biochemistry and Molecular Biology, Pennsylvania State University, University Park, PA 16802, USA

^b Department of Chemistry, Marquette University, Milwaukee, WI 53233, USA

^c Department of Chemistry, University of Akron, Akron, OH 44325, USA

d Department of Chemistry, Emory University, Atlanta, GA 30322, USA

^e Department of Chemistry, Pennsylvania State University, University Park, PA 16802, USA

f The Huck Institutes of the Life Sciences, Pennsylvania State University, University Park, PA 16802, USA

^{*} Corresponding author at: Department of Biochemistry and Molecular Biology, Pennsylvania State University, University Park, PA 16802, USA.

^{**} Corresponding author at: Department of Chemistry, University of Akron, Akron, OH 44325, USA.

^{***} Corresponding author.

E-mail addresses: james.kincaid@marquette.edu (J.R. Kincaid), yliu1@uakron.edu (Y. Liu), emily.weinert@psu.edu (E.E. Weinert).

¹ These authors contributed equally to this work.

 $^{^{2}}$ Deceased.

DGC domains must dimerize to synthesize c-di-GMP. Furthermore, the oligomerization state of some DGC-containing GCS proteins varies; some GCS proteins, such as from Escherichia coli (EcDosC), form dimers in vitro, while GCS from Bordetella pertussis (BpeGReg) and Pectobacterium carotovorum (PccGCS) form mixtures of primarily low activity dimers and high activity tetramers, and Desulfotalea psychrophile (HemDGC) forms homotetrameric assemblies. In addition, binding of c-di-GMP to the inhibitory site (I-site), which decreases diguanylate cyclase activity through feedback inhibition, can shift the ratios of oligomeric state for PccGCS and BpeGReg. Oligomerization state of DGC-containing GCSs may be due to differences in amino acid sequence, as mutation of Bpe-GReg and PccGCS I-site residues alters oligomerization state, or could be due to interactions with other cellular proteins. For example, EcDosC is co-transcribed and translated with EcDosP, a c-di-GMP phosphodiesterase, in cellulo and the two proteins form a hetero-oligomer when expressed and purified from E. coli, while PccGCS has not been found to strongly interact with other cellular proteins. These differences between DGC-containing proteins could result in different signal transmission mechanisms, supporting the need for further studies to identify residues involved in signaling and putative inter-domain interactions.

Much of the previous work on the intra-protein signal transduction mechanism has been developed from the crystallized globin domains of GCS proteins, including the sensor globin domains from *Bacillus subtilis* (HemAT-*Bs*) [12], *EcDosC* [13], *Anaeromyxobacter* sp. strain Fw109–5 (*Af*GcHK) [14,15], and *Bpe*GReg [16]. These structures and accompanying biochemical studies have suggested three heme pocket residues as the major contributors to the signaling mechanism: the primary hydrogen bond-donating distal Tyr, a secondary distal H-bond donor (Ser or Thr), and the proximal His that ligates the heme iron center (Fig. 1) [17–19]. Given the importance of the three heme pocket residues in stabilizing ligand binding, it has been hypothesized that the residues would be involved in the intra-protein signaling mechanism of GCSs.

A recent crystal structure of the globin domain from the DGC-GCS BpeGReg (BpeGlobin) highlighted additional structural features potentially involved in O2-dependent signaling of GCS proteins [16]. In particular, comparison of BpeGlobin structures in the Fe(II)-O2 (cyclase "on" state) and Fe(III) (cyclase "off" state) ligation states suggested a mechanism in which the signal is propagated through interactions between a distorted heme cofactor and heme edge residues, particularly a tryptophan residue on the E helix, which formed a T-type π -stack with the heme cofactor. In addition, the GCSs from Paenibacillus dendritiformis (bifunctional DGC-phosphodiesterase output domains, DcpG) and Bacillus subtilis (methyl accepting chemotaxis protein output domain, HemAT-Bs) contain a histidine residue and exhibit markedly weaker O2 affinity [12,20-22], suggesting a role for the heme edge residue in modulating enzyme characteristics. Previous studies identified crosslinks between the sensor globin domain and the diguanylate cyclase domain, as well as π -helix within the middle domain that is involved in

cyclase domain activation, suggesting a potential mechanism for transmitting changes in heme pocket residue conformation to control output domain activity. To probe the role of the heme pocket in modulating enzyme activity, the DGC-GCS from the bacterial soft rot pathogen *Pectobacterium carotovorum* (*Pcc*GCS), which is similar in length and domain organization to *Bpe*GReg [2,17], was interrogated. Using a combination of resonance Raman spectroscopy, enzyme kinetics, analytical ultracentrifugation, and small angle X-ray scattering (SAXS), we have generated a full-length models of tetrameric *Pcc*GCS and variants and demonstrated that *Pcc*GCS heme edge residues modulate ligand-dependent activation of DGC-GCS proteins and control DGC domain conformation.

2. Materials and methods

2.1. Protein expression

Site-directed mutagenesis was performed on a codon-optimized gene encoding PccGCS within a pET-20b vector [2]. Primers used for mutagenesis can be found in Supporting Information Table S1. Protein variants were generated by standard PCR protocol as previously described [17]. Proteins were expressed in E. coli Tuner (DE3) pLysS cells (Novagen) as previously described [17,23]. Briefly, cells were transformed with pET20b plasmids encoding each protein via heat shock, then grown overnight on LB agar plates containing chloramphenicol (30 µg 1/mL) and ampicillin (100 µg 1/mL). Plates were restreaked and single colonies were selected and grown overnight at 37 °C with shaking at 225 rpm in lysogeny broth (LB) medium with appropriate antibiotics for selection. These overnight cultures were then used to inoculate globin expression media (45 g yeast extract, 10 mL glycerol, 2.31 g anhydrous KH₂PO₄, 12.54 g anhydrous K₂HPO₄ per 1 L of ultrapure water). The inoculated cultures were incubated at 37 °C with shaking at 225 rpm until they reached an OD₆₀₀ of 0.6-0.8. At this point, the temperature was decreased to 25 $^{\circ}\text{C}$ and δ -aminolevulinic acid was added at a final concentration of 500 µM to each expression mixture. Cultures were incubated with shaking for 30 min, at which point protein expression was induced by addition of 100 μM IPTG for 6 h. Cells were then harvested by centrifugation (3500 xg, 4 °C, 20 min) and the resulting pellets were collected and stored at -80 °C.

2.2. Protein purification

Low imidazole buffer (50 mM Tris, 50 mM NaCl, 1 mM DTT, 20 mM imidazole, pH 7.0) was used to resuspend cell pellets, which were then lysed using a homogenizer (Avestin) or a sonicator (Qsonica), and partially purified by centrifugation (186,000 xg, 4 $^{\circ}$ C, 1 h). The resulting supernatant was then loaded onto an equilibrated HisPur Ni²⁺-column (Fisher Scientific) and washed with low imidazole buffer. The protein was eluted using high imidazole buffer (50 mM Tris, 50 mM NaCl, 1 mM

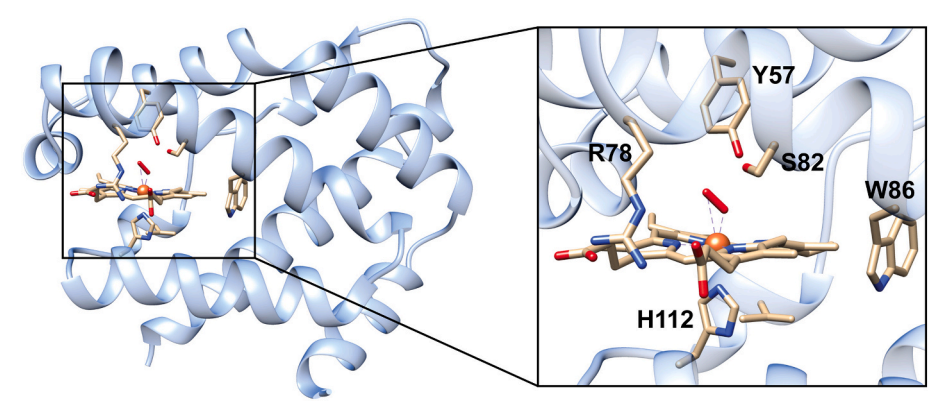


Fig. 1. Homology model of PccGCS globin domain and heme pocket with key residues labeled.

DTT, 250 mM imidazole, pH 7.0) and, following elution, proteins were further purified and desalted with a S200 gel filtration column (GE Healthcare; Buffer A: 20 mM HEPES, 50 mM NaCl, 1 mM DTT, 2.5% glycerol (ν / ν), pH 7.0). Protein-containing fractions were then concentrated by ultrafiltration (10 kDa MWCO filter, Millipore), aliquoted, flash frozen in liquid nitrogen, and stored at $-80\,^{\circ}$ C.

2.3. Michaelis-Menten enzyme kinetics

Proteins were reduced and various protein ligand complexes were formed prior to kinetic assays as previously described [24–26]. Ligation states were verified for each protein via UV–vis spectroscopy prior to each assay. All Fe(II) and Fe(II)-NO kinetic rates were measured in an anaerobic chamber (Coy). In order to measure the rates of DGC output from the DGC-GCS proteins, the EnzChek pyrophosphate kit (Life Technologies) was used according to the manufacturer's instructions, the exception being that a phosphodiesterase (PDE) EcDosP was added in 3-M excess to eliminate product inhibition [11] and the reactions were initiated by the addition of varying concentrations of GTP. Assays were performed in triplicate in 96-well plates with 4 protein concentrations (0, 0.5, 1, and 2 μ M) and 4 GTP concentrations (0, 100, 250, and 1000 μ M) and were monitored using an Epoch or Epoch2 plate reader and Gen5 software (Biotek) and repeated at least twice to account for day-to-day variability.

2.4. Stopped-flow kinetics

 O_2 dissociation rates were performed as previously described [17,26]. Briefly, all proteins were reduced with dithionite in an anaerobic chamber (Coy), desalted into anaerobic Buffer A (50 mM Tris, 50 mM NaCl, 1 mM DTT, pH 7.0), and then mixed with O_2 saturated Buffer A to yield final concentrations of 5–10 μ M. Protein samples were rapidly mixed with a solution of sodium dithionite in Buffer A (final dithionite concentration = 5 mM; dithionite concentration of 0.5 mM also was tested and dithionite concentration was found to not affect the O_2 dissociation rate) in an SX20 stopped flow apparatus. The dissociation of O_2 performed at 25 °C was monitored using the SX20 stopped flow equipped with a diode array detector and temperature-controlled bath and fit globally using Pro-KII software (Applied Photophysics). Additional fitting analysis was performed using Igor Pro (Wavemetrics).

2.5. Resonance Raman spectroscopy

To prepare the deoxygenated samples, PccGCS WT, W86H and R78G (\sim 100 μ L of 120 μ M) were placed in NMR tubes (WG-5 M-ECONOMY-7, Wilmad Glass Co., Beuna, NJ), connected to a vacuum line and degassed followed by saturation with argon gas. This procedure was repeated twice. Sufficient dithionite solution was added to fully reduce the samples, the formation of ferrous form was confirmed by monitoring the Q region of electronic absorption spectrum, using a device (ISS-2 integrated sampling system, Ocean Optics Inc) that can measure spectra for the NMR tubes connected to vacuum line. To prepare the oxygenated samples, approximately 10 mL of oxygen gas ($^{16}O_2$ or $^{18}O_2$) was added with a gas tight syringe to the ferrous PccGCS solutions to form the oxy complexes. The samples were gently shaken for 10s followed by rapid freezing in a liquid nitrogen bath.

The rR spectra of ferrous forms were acquired with the 441.6 nm line from a He—Cd laser (1 K Series He—Cd laser, Kimmon Koha., Ltd), while the oxygenated samples were measured using 413.1 nm excitation line, which is from a Kr + laser (Coherent Innova Sabre Ion Laser). All spectra were measured using a Spex 1269 spectrometer equipped with a Spec-10 LN liquid nitrogen-cooled detector (Princeton Instruments, NJ). The rR spectra were collected using back scattering (180°) geometry with the laser beam being focused by a cylindrical lens to form a line image on the sample to help prevent heating and minimize photodissociation. The laser power incident on the ferrous samples was maintained at $\sim\!10$ mW,

while being adjusted to 1 mW or less on the oxygenated samples. The slit width was 150 µm and the 1200 g/mm grating was used for measurements. Spectra were calibrated with data acquired for fenchone and processed with Grams/32 AI software (Galactic Industries, Salem, NH).

2.6. Small-angle X-ray scattering (SAXS)

Samples of PccGCS wild type (WT) and H237A/K238A variants were prepared in Buffer A and concentrations of 100 µM and 183 µM, respectively. All samples were centrifuged at 14,000 rpm for 10 min to minimize aggregation and to remove dust particles prior to inline size exclusion chromatography (SEC). Synchrotron SAXS data with inline SEC were collected at the macromolecular Cornell High Energy Synchrotron Source, MacCHESS, on the G1 beamline station. Chromatographic separation of samples was conducted at 4 °C using Superdex 200 5/150 and 10/300 columns on an AKTA Pure system (GE Healthcare Life Sciences, Marlborough, MA). Sequential 1 s (5/150) or 2 s (10/300) exposures with flow rates of 0.15 (5/150) to 0.5 (10/300) mL/min were used. Synchrotron beam was centered on a capillary sample cell with 1.5 mm path length and 25 µm thick quartzglass walls (Charles Supper Company, Natik, MA). The sample cell and full X-ray flight path, including beam stop, were kept in vacuo ($< 1 \times 10$ –3 Torr) to eliminate air scatter. Temperature was maintained at 4 °C. Data were collected at 293 K using a dual PILATUS 100 K-S SAXS/WAXS detector and a wavelength of 1.264 Å. The sample capillary-to-detector distance was 1508.0 mm and was calibrated using silver behenate powder (The Gem Dugout, State College, PA). The useful q-space range $(4\pi \text{Sin}\theta/\lambda \text{ with } 2\theta)$ being the scattering angle) was generally from qmin = 0.008 Å-1 to gmax = 0.27 Å-1 ($q = 4\pi \sin(\theta)/\lambda$, where 2 θ is the scattering angle). The energy of the X-ray beam was 9.808 keV, with a flux of 3 \times 10 **11 photons/s and a diameter of 250 $\mu m \times 250~\mu m$. The synchrotron storage ring was running at 50 milliamps positron current.

The BioXTAS RAW software was used at the synchrotron for the SEC data collection, data reduction and background buffer data subtraction (Fig. S2A) [27]. Image integration, normalization, and subtraction was carried out using the RAW program. Radiation damage was assessed using the CORMAP criterion as implemented in RAW's built-in averaging function. Sample and buffer solutions were normalized to equivalent exposure before subtraction using beamstop photodiode counts. The forward scattering I(0) and the radius of gyration (R_g) were calculated using the Guinier approximation, which assumes that at very small angles ($q < 1.3/R_g$) the intensity is approximated as $I(q) = I(0)\exp[-1/3(qRg)^2]$. The molecular mass was estimated using a comparison with glucose isomerase and lysozyme standard protein data in the RAW software.

Protein samples of bovine serum albumin were used as the standard in both the SEC-MALS and the in-house SAXS molar mass measurements. Samples of GCS R78G and W86H variants were prepared in Buffer A and concentrations of 127 μM and 85 μM, respectively. ~700 μg of protein was separated into 200 µL fractions using an Agilent 1260 Infinity II HPLC system equipped with a 300 Å SEC Analytical Column at 20 °C to purify tetrameric protein, with the Buffer A as the mobile phase (0.5 mL/ min). Molar mass of tetrameric complexes were confirmed using an inline Wyatt Technology DAWN MALS and Wyatt Optilab Refractive Index (RI) detector. SAXS data was collected at 1.54 Å using a Rigaku MM007 rotating anode X-ray generator and a BioSAXS2000nano Kratky camera system. The system includes OptiSAXS confocal max-flux optics and a sensitive HyPix-3000 hybrid photon counting detector. The sample capillary-to-detector distance was 495.6 mm and was calibrated using silver behenate powder (The Gem Dugout, State College, PA). The samples of PccGCS were loaded using an autosampler onto a quartz capillary flow cell mounted on a stage cooled to 20 $^{\circ}\text{C}.$ The sample cell and full X-ray flight path, including beam stop, were kept in vacuo (< 1mTorr) to eliminate air scatter. Data reduction including image integration, normalization, and background buffer data subtraction were performed with the Rigaku SAXSLAB software.

For both synchrotron and in-house SAXS data analysis, the software suite ATSAS [28] was used. Kratky plots indicated that the protein was well folded and with no disorder (Fig. S2B). GNOM [29] was used to calculate the pair-distance distribution function P(r), from which the maximum particle dimension (Dmax) and Rg were determined (Fig. S1, S2, Table S2). Ab initio low-resolution solution models were reconstructed using DAMMIN [30] for data in the range (0.00699 $< q < 0.3563 \ {\rm \AA}^{-1}$). Twenty models were generated from each program and averaged using DAMAVER [31]. The normalized spatial discrepancy parameter (NSD) obtained from DAMAVER indicated the similarity between models used for average calculations. NSD values ≤ 1.0 were obtained as expected for similar models (Fig. 4 A). The theoretical scattering profiles of the constructed models were calculated and fitted to experimental scattering data using CRYSOL (Fig. S3).

Individual domains of the PccGCS structures, globin, mid and cyclase domains were generated using homology modelling in the Swissmodel software [32]. Possible tertiary and quaternary structures of globin, middle domain, and cyclase dimers were modeled manually in Pymol graphics software [33] guided by the available high resolution protein structures (DGC 4URG [34], globin 6I2Z [35], middle 4ZVC [13]). The complete PccGCS dimer model hence built was energy minimized using the Chimera software [36]. To evaluate the conformational flexibility of the domains in the manually fit tetramer, SREFLEX [37] software was used with the individual dimers refined as independent rigid bodies. This ATSAS program uses normal mode analysis to estimate the flexibility of high-resolution models and improves their agreement with experimental small angle X-ray scattering (SAXS) data. The theoretical scattering was calculated for each generated model by CRYSOL. The Chi**2 fit for the PccGCS tetramer generated for the WT and variants was close to 1, supporting the robustness of the SAXS models. Final models for each variant were substantially different than the WT solvent envelope, supporting the differences in conformation (Fig. S4).

2.7. Multiwavelength analytical ultracentrifugation

The Optima AUC data for PccGCS wild type and variants R78G and W86H proteins were obtained at concentrations of $\sim\!5~\mu\text{M}$ to give sufficient signal. Protein ligation states were generated as described above. For anaerobic experiments, the cells were brought into the anaerobic chamber and and flushed with ambient air in the chamber before equilibration for $\sim\!16\text{--}24~h$ prior to loading the proteins. The monitoring utilized three wavelengths: 280 nm, 414 nm, and 430 nm absorbance. The run was conducted at 20,000 RPM in 12 mm titanium centerpiece cells with sapphire windows. For anaerobic runs, the centerpiece cells were loaded in a Nitrogen glove box and tightly sealed before transfer to the Optima. The rotor used for both aerobic and anaerobic runs was a TI-60 titanium 4-hole rotor, pre-equilibrated to a run temperature of 20 °C. The run duration was 17 h, with multiwavelength scans taken at 2-min intervals. Ultrascan software refinement was applied for Optima multiwavelength data analysis.

The data was analyzed as a pseudo-3-dimensional distribution, with the calculated molecular weight on the x-axis, the calculated frictional ratio on the y-axis, and the % concentration in the Z-plane, with the heat map on the right axis. The heat map scale varies depending on the highest signal observed in each sample (Fig. S6). Across all tested conditions, the molecular weight consistently approximates that of a tetrameric species. The conformational states of PccGCS under various conditions are elucidated in the frictional ratio 2D-plots (Fig. S6). Frictional coefficients provide insights into the shape of the molecule; a perfect sphere yields a coefficient of 1, and the larger the coefficient, the greater the deviation from a sphere. Collectively, the numerous variants and wild type of PccGCS in both aerobic and anaerobic environments exhibit multiple distinct frictional coefficient (f/f_0) values at the approximate MW of the tetramer (\sim 220 kDa), each associated with a unique tetramer conformation.

3. Results and discussion

3.1. Effects of heme pocket mutations on O2 binding

Previous work has established that GCS proteins often serve as O2 sensors, with O2 binding resulting in increased diguanylate cyclase activity [2,4,11,18] and that residues within the heme pocket are involved in the GCS signaling mechanism and modulation of ligand binding affinity [16-18]. Therefore, the O2 dissociation rates of PccGCS variants were obtained to link the roles of heme pocket residues in signaling to their roles in O2 binding (Table 1). Both variants fully bound O2, as assessed by UV-visible spectra (spectra are the same as PccGCS WT [38] and other PccGlobin variants [17]), which was expected based on the O2 association rate for *PccGCS* WT (7.2 μ M⁻¹ s⁻¹; calculated K_D s = 78 and 538 nM [17]). The two variants also exhibit two O₂ dissociation rates, as previously observed for PccGCS WT, which have been attributed to differences in hydrogen bonding interactions within the pocket [16,17]. HemAT-Bs also exhibits two O2 dissociation rates that were correlated with hydrogen bonding patterns between the bound O2, distal pocket tyrosine and serine residues, and an ordered distal pocket water [19,22,39]. The PccGCS W86H variant, which was generated to mimic the heme edge histidine in HemAT-Bs [39] (H99) and DcpG (H62) [21], exhibited increased O2 dissociation rates, as compared to PccGCS WT. Previous studies have demonstrated that HemAT-Bs and DcpG exhibit rapid O2 dissociation [22], suggesting that the identity of the aromatic residue at this position is important for O2 stability. The W86 position does not directly interact with the bound ligand in crystal structures of sensor globins [12,13,15,16,39]; however, the residue is within Van der Waals contact of the heme, suggesting that this position is important for modulating O₂ binding. In contrast, the R78G variant, which should eliminate hydrogen bonding to a heme propionate, did not have a significant effect on O2 dissociation.

3.2. Heme pocket residues control DGC activation

In order to investigate the role of heme pocket residues in DGC activation, enzyme kinetic assays were performed on PccGCS WT and variants in the unbound (Fe(II)), ferrous-oxy (Fe(II)-O2), and ferrousnitric oxide (Fe(II)-NO) forms. PccGCS WT was assayed as a control and Fe(II) and Fe(II)-O₂ K_M and k_{cat} values were the same as previously reported (Table 2) [2,17]. The PccGCS W86H variant, which mimics the heme edge residue found in HemAT-Bs [39] and DcpG [21], exhibited increased DGC activity in all ligation states, as compared to PccGCS WT. Furthermore, the fold-change in k_{cat} (Fe(II)-O₂/Fe(II) \sim 5) for the W86H variant is twice that of PccGCS WT (Fig. 2), indicating that W86 is a major modulator of cyclase activation in these proteins. The PccGCS R78G variant, however, exhibited a 2-fold increase in Fe(II) activity and no longer displayed ligand-dependent cyclase activation. The failure of the R78G variant to exhibit ligand-dependent activation is striking because this position was shown to make a hydrogen-bond with the heme C-ring propionate in the Fe(II)-O2 monomers of the BpeGlobin crystal structure, but not the Fe(III) form. This suggests that liganddependent movements of heme propionates could lead to larger conformational changes in the protein by means of R78 hydrogen bonding. Both variants also exhibit the increased activation for O₂ vs. NO, despite the higher affinity of NO for histidyl ligated heme proteins [40], as previously was observed for PccGCS WT [38]. The O2 selectivity suggests that specific hydrogen bonding interactions [19,41] between

Table 1Oxygen Dissociation Rates. All measured errors are <5%.

Protein	k_1	k_2	$\% k_1$	$\% k_2$
PccGCS WT [38]	0.56	3.87	56	44
PccGCS R78G	0.57	4.54	76	24
PccGCS W86H	1.35	6.08	42	58

 Table 2

 PccGCS diguanylate cyclase kinetic parameters.

	Fe(II)			Fe(II)-O ₂			Fe(II)-NO		
Protein	k_{cat} (min ⁻¹)	$K_{ m M}$ (μ M)	$k_{\text{cat}}/K_{\text{M}}$ $(M \bullet \min)^{-1}$	k_{cat} (min ⁻¹)	<i>K</i> _M (μM)	$k_{\text{cat}}/K_{\text{M}}$ $(\text{M}ullet \text{min})^{-1}$	k_{cat} (min ⁻¹)	<i>K</i> _M (μM)	$k_{\text{cat}}/K_{\text{M}}$ $(\text{M} \bullet \text{min})^{-1}$
WT ²	0.29 ± 0.01	62 ± 3	4677	0.73 ± 0.01	31 ± 6	23,548	0.51 ± 0.01	32 ± 5	15,938
R78G	0.74 ± 0.09	93 ± 1	7957	0.72 ± 0.03	104 ± 31	6923	0.65 ± 0.1	87 ± 7	7471
W86H	0.45 ± 0.01	193 ± 30	2332	2.33 ± 0.05	23 ± 6	101,304	1.02 ± 0.3	52 ± 8	19,615

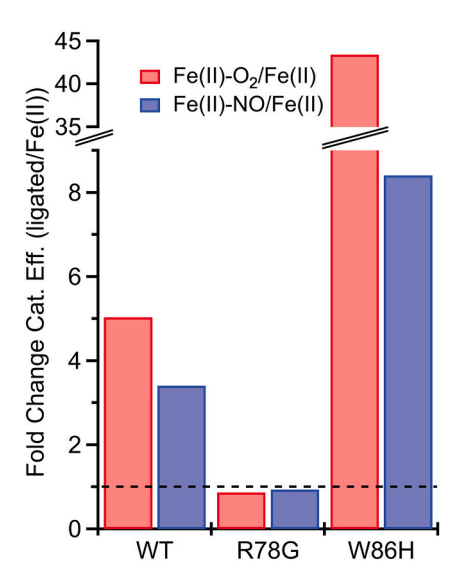


Fig. 2. Comparison of the ratios of PccGCS catalytic efficiencies in Fe(II)-ligated vs. Fe(II)-unligated states. Fold-change of 1 (no change between ligation states) is shown as a dotted line.

distal pocket residues and the bound $\ensuremath{O_2}$ are required for full cyclase domain activation.

3.3. Comparison of PccGCS WT and variants using resonance Raman spectra

As the PccGCS W86H and R78G variants showed significant changes in cyclase activity, resonance Raman (rR) spectroscopy was used to characterize changes in heme conformation and properties. The rR spectra of ferrous forms of the PccGCS WT, W86H and R78G variants exhibit similar spectra in both low and high frequency regions (Fig. 3). In Fig. 3 A (right panel), the high-frequency rR spectrum of WT PccGCS confirms the presence of a pure ferrous form (oxidation state marker at 1354 cm⁻¹) and the spin state markers, ν_3 , ν_2 and ν_{10} modes, are observed at 1473, 1570 and 1612 cm⁻¹, respectively, indicating a pure five-coordinated high spin species (5cHS). The mode occurring at 1623 cm⁻¹ is most reasonably assigned as the vinyl ν (C=C) mode. Mutating the bulky W86 residue to His does not induce any significant changes, as seen in Fig. 3B (right panel); the rR spectrum exhibits characteristics of a 5cHS species, i.e., the ν_3 , ν_2 and ν_{10} modes occur at 1475, 1570 and 1612 cm⁻¹. It is noted that the vinyl stretching mode is observed at 1625 ${\rm cm}^{-1},$ quite similar to that of the WT protein. Similarly, the rR spectrum of ferrous R78G (Fig. 2C, right panel) exhibits the same heme markers as the wild-type and is assigned to the 5cHS species.

The low frequency region rR spectra can provide useful information regarding the bending motions of the heme peripheral groups, out-of-plane (oop) modes activated by distortions of heme macrocycle, and detailed information on H-bonding interactions of bound diatomic molecules with distal pocket H-bond donor residues [19,42–45], all of which can significantly impact heme protein functional properties [46–49]. Typically, the propionate bending modes are observed in the

region of \sim 360–380 cm⁻¹, where the higher frequency bending mode is associated with stronger H-bonding between the carboxy group with the nearby amino acid residues [48,50,51]. Furthermore, the vinyl modes usually occur in the region of ~400-440 cm⁻¹, where the lower frequency indicates a nearly planar orientation relative to the pyrrole rings, and the higher frequency is associated with a more out-of-plane orientation respect to the pyrrole ring of the macrocycle [49,52]. Fig. 3 A (left panel) shows the low frequency rR spectrum of WT PccGCS; the heme skeletal modes for WT *PccGCS* are assigned as ν_7 (670 cm⁻¹), ν_{15} (754 cm⁻¹), and ν_8 (340 cm⁻¹). The propionate modes are observed at 363 and 377 cm⁻¹, and the vinyl mode is at 410 cm⁻¹. Prominent out-ofplane (OOP) modes are seen at 305, \sim 487, 545 and 714 cm⁻¹, assigned to the γ_7 , γ_{12} , γ_{21} and γ_{15} modes, manifestation of these modes being characteristic of a "doming" oop distortion of the heme macrocycle typically seen for deoxy globins [53]. The strongly enhanced proximal ν (Fe-N_{his}) mode is observed at 229 cm⁻¹; the position of this mode depends on different factors, including the H-bonding to the proximal His N^{δ} hydrogen, the effect of strain from the protein on the Fe-Nhis bond, and geometry of bound imidazole. As summarized in Table 3, Cytochrome c peroxidase has a very high Fe-Nhis stretching mode at 245 cm⁻¹, which is attributable to the strong hydrogen bond between the axial His and Asp235, increasing the basicity of the proximal histidylimidazole fragment. On the other hand, the Hemoglobin T and R states show distinguishable differences in the v(Fe-Nhis) stretching frequencies, the lower frequency observed (215 cm⁻¹) for the T state being a consequence of the strain in the T quaternary structure. Accordingly, the higher vibrational frequency of the Fe-N_{his} mode in deoxy *Pcc*GCS is indicative of less strain being imposed on the Fe- N_{his} bond or possibly suggests interaction of the histidyl imidazole with a relatively basic proximal pocket residue. However, as no interactions were observed between the histidyl imidazole and either side chains or backbone amides in the crystal structure of B. pertussis globin [16], the higher frequency of the Fe-N_{his} mode is likely due to lower strain.

As shown in Fig. 3B (left panel), it is interesting to see that the W86H mutation does not cause any significant changes in the heme skeletal and oop modes or the vinyl bending mode (410 cm $^{-1}$); both PccGCS WT and W86H vinyl groups adopt the more in-plane orientation, suggesting an enhanced conjugation. Similarly, the propionate bending mode region indicates that the prominent mode at 363 cm $^{-1}$ is not altered, while the higher frequency mode (374 cm $^{-1}$) is slightly weaker and downshifts by 3 cm $^{-1}$ upon mutation, implying that hydrogen bonding to the propionate groups is potentially slightly weakened in the W86H variant. It is important to note that the ν (Fe-N $_{\rm his}$) mode still occurs at 229 cm $^{-1}$, indicating that mutation at Trp86 does not affect the Fe-N $_{\rm his}$ bond on the proximal side.

In contrast, the ferrous state rR spectra of R78G mutant (Fig. 3C) reveals a 4 cm $^{-1}$ downshift of the $\nu(\text{Fe-N}_{\text{His}})$ stretching wavenumber (225 cm $^{-1}$), as compared to PccGCS WT and W86H variant (229 cm $^{-1}$). This implies that the strength of the proximal heme Fe-N_{His} linkage is weakened upon introduction of the R78G mutation, probably caused by the conformational change that results in a flexible active site and a relatively labile Fe-N_{His} bond. However, there are no significant differences in alterations to the geometry of heme peripheral groups or activation of out-of-plane modes that would reflect varying degrees of heme ruffling. In summary, these rR studies of the ferrous states suggest very small changes in heme structure for the W86H varient, but mutating the

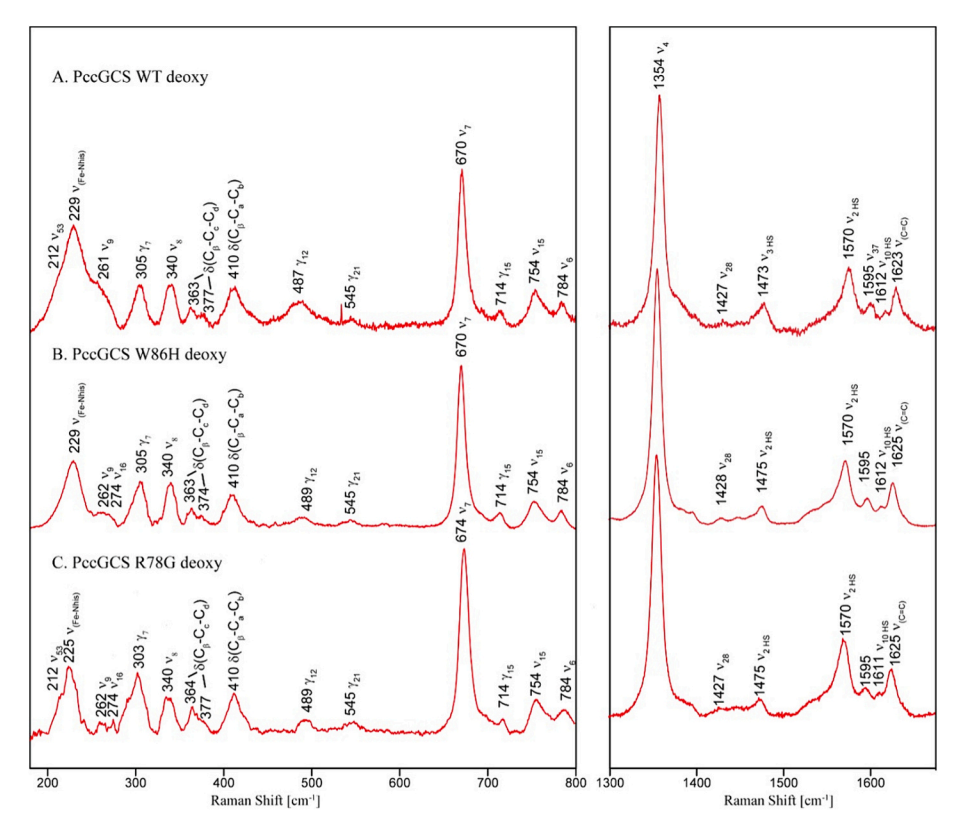


Fig. 3. rR spectra of deoxy PccGCS. The rR spectra of deoxy PccGCS (A), W86H mutant (B) and R78G mutant (C). Spectra were obtained using 441.6 nm excitation line. The left panel is in low frequency region, while the right panel is for high frequency. It is noted that the key ν (Fe-N_{his}) mode of PccGCS WT appearing near 229 cm⁻¹ is more intense that that observed for the mutant; this is likely due to the presence of excess aqueous dithionite used to reduce these proteins, a species which exhibits a strong band at 228 cm⁻¹ along with a moderately intense feature near 460 cm⁻¹. Additional intensity in the rR spectrum of the WT protein as also detected near 460 cm⁻¹.

 $\begin{tabular}{ll} \textbf{Table 3} \\ \textbf{Summary of observed Fe-N}_{his} \ \textbf{Frequencies in different heme proteins.} \\ \end{tabular}$

	ν (Fe-N _{his})	Ref.
Native deoxy Myoblobin	$220 \; {\rm cm}^{-1}$	[54]
deoxy Hemoglobin (T state)	215 cm^{-1}	[55]
deoxy Hemoglobin (R state)	221 cm^{-1}	[55]
ferrous HRP at pH = 8	241 cm^{-1}	[56]
ferrous HRP at pH = 5	244 cm^{-1}	[56]
Cytochrome c peroxidase	$245 \; {\rm cm}^{-1}$	[57,58]

distal R78 residue induced slight conformational changes in the proximal active site.

Considering the suggested importance of heme edge residues in controlling both O2 affinity and cyclase activation in DGC-GCS proteins, characterizing the oxy ferrous intermediates of the WT and W86H mutant is particularly useful. As seen by comparing the spectral traces shown in panels A and B of Fig. 4, while PccGCS WT retains low frequency oop modes (γ_6 , γ_7 , γ_{12} and γ_{21}), the W86H mutation causes substantial decreases in the number and intensities of these oop modes, as compared to the WT protein. As the flattening of the macrocycle in the oxy form compared to the deoxy form is correlated with activation of cdi-GMP production, the rR data are consistent with the W86H variant increased activity being due to its less distorted oxy form heme. However, there are other substantial differences in the rR spectra of these two proteins which suggest other possible control mechanisms. From the $^{16}{\rm O}_2-^{18}{\rm O}_2$ difference spectra of the oxy samples of *Pcc*GCS WT (Fig. 4, traces D and E), a clearly observed positive band at 568 cm⁻¹ downshifts by 25 cm⁻¹ upon ¹⁸O₂ substitution. This mode has been assigned to the Fe—O stretching mode and the isotope shift is in good agreement with a calculated shift value of 25 cm⁻¹. A related globin coupled sensor,

BpeGReg, exhibits only a single closed conformation which binds oxygen tightly, with the Fe—O stretching mode occurring at 560 cm⁻¹ [35]. BpeGReg, like PccGCS, contains a heme edge tryptophan residue, W72, which formed a T-type π -stack with the heme cofactor [16]. It has been suggested that the signal transduction is propagated through interactions between a distorted heme cofactor and this particular heme edge residue. Interestingly, in the present case (Fig. 4D) the PccGCS W86H variant provides clear evidence that the heme macrocycle is flatter than that for the WT protein, with many fewer oop modes being present. Moreover, it is also quite clear that there are distal pocket rearrangements, with the W86H variant showing three separate ν (Fe—O) modes observed at 578 cm⁻¹, 572 cm⁻¹ and 566 cm⁻¹, respectively (with isotopic shifts being reasonable consistent with predicted values). Based on comprehensive work by Spiro and coworkers [42] and data analyzed for a series of oxy complexes of cytochromes P450 [59-62], these varied frequencies are interpreted to represent different hydrogen bonding interactions with H-bond donors in the distal pocket of the W86H mutant. The central ν (Fe—O) stretching mode at 572 cm⁻¹ corresponds to the non-hydrogen bonded form, whereas the mode appearing at 578 cm⁻¹ indicates the presence of H-bonding with the terminal O atom of heme-bound O₂, while the frequency at 566 cm⁻¹ suggests H-bonding to the proximal O atom. Interestingly, Kitagawa et al. first demonstrated the presence of three different conformers in the wild-type O₂ bound form of HemAT-Bs [19], where the oxygen isotope sensitive bands were observed at 554, 566, and 572 cm⁻¹ [19], designated as the closed form, open α form, and open β form, respectively. As HemAT-B has a heme edge residue (His99) positioned precisely where H86 occurs in the PccGCS W86H mutant [12], our work suggests that this heme edge residue replacement plays a key role in affecting the Hbonding network on the distal ligand binding side of the heme, generating multiple conformations of the Fe-O-O fragment.

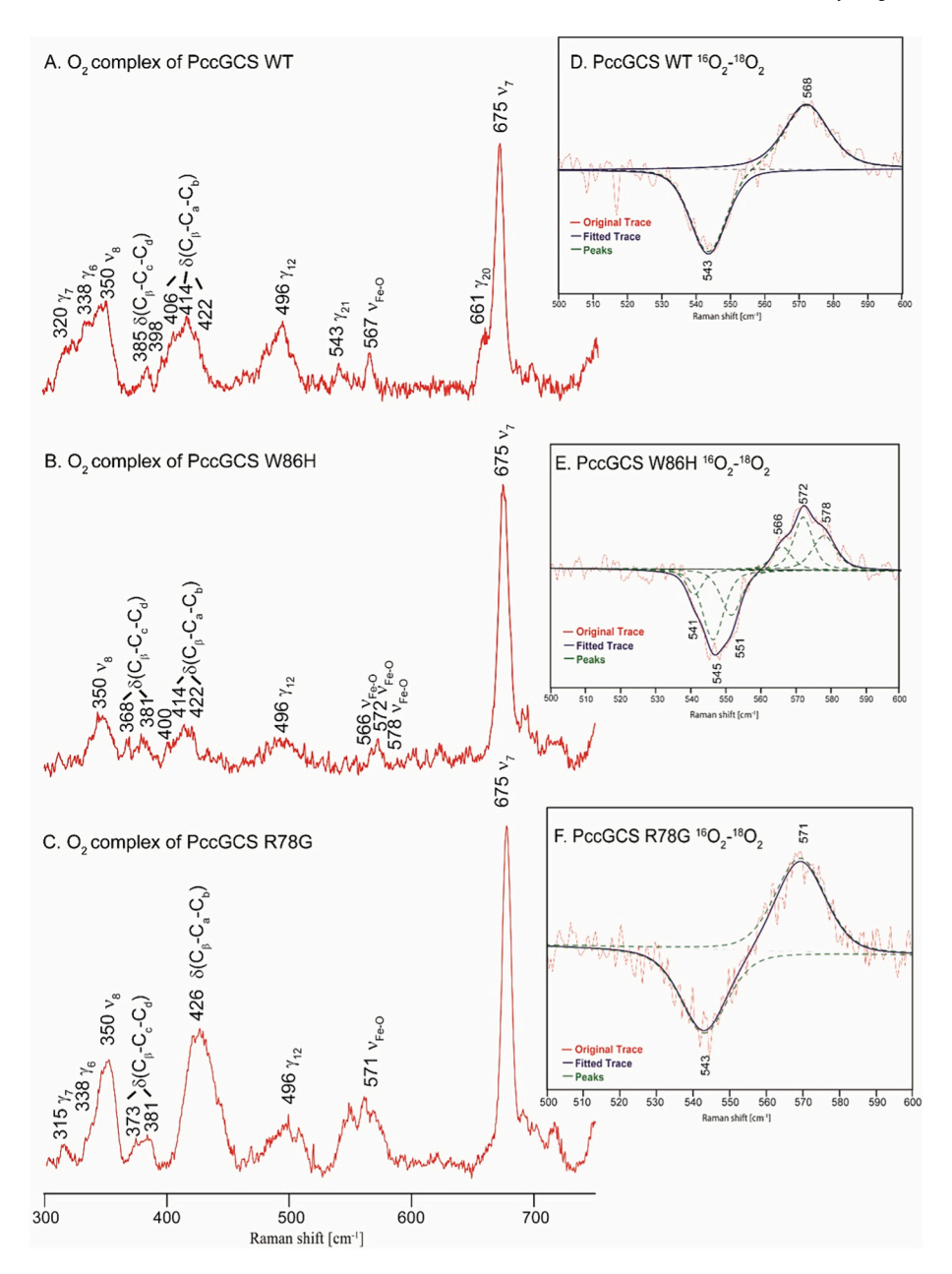


Fig. 4. rR spectra of oxy PccGCS. The rR spectra of oxy PccGCS (A), W86H mutant (B) and R78G mutant (C). Spectra were obtained using 413 nm excitation line. The inset shows the $^{16}\text{O}_2$ - $^{18}\text{O}_2$ difference traces of WT PccGCS (D), W86H PccGCS (E) and R78G PccGCS (F). Spectra were deconvoluted with Grams 32/AI software using a peak fitting procedure, employing 50/50% Gaussian/Lorentzian functions. Red solid line, experimental data; blue solid line, fitted spectra; green dotted line, modes associated with ν (Fe—O) modes.

To understand why the R78G variant does not exhibits ligand-dependent activation, the oxy complex of PccGCS R78G mutant was prepared and analyzed by rR spectroscopy. Comparing the oxy rR spectrum of R78G with the WT (Fig. 4 A and 4C), the R78G mutation was found to result in a less ruffled heme, as reflected in the deactivation of several out-of-plane modes in the low-frequency region (intensity of γ_6 and γ_7 are decreased compared to the WT and the γ_{21} mode disappeared in the R78G variant). It has been suggested that heme flattening is important for signal transduction in H-NOX family [63,64] and our observation of a flatter heme in the more active PccGCS W86H variant suggests that heme flattening is also involved in GCS signal transduction. Most interestingly, significant alterations to the geometry of heme peripheral groups are observed in R78G mutant. The mutation causes an activation of the 373 cm $^{-1}$ bending mode of propionate group, indicating structural reorientation and a perturbed hydrogen bonded

propionate group. Such observations are in good agreement with the crystallographic data, which found that this position forms a hydrogenbond with heme C-ring propionate in the Fe(II)-O₂ monomers of the *Bpe*Globin crystal structure [16]. Moreover, the rR spectral data obtained here provide definitive evidence that mutation R78 residue causes active site perturbations that generate more out-of-plane vinyl groups, as reflected by the increased intensity of vinyl bending mode observed at 426 cm⁻¹. In the 16 O₂— 18 O₂ difference spectra obtained for oxy R78G *Pcc*GCS (Fig. 3F), the ν (Fe—O) mode is observed at 571 cm⁻¹ and shifts by 28 cm⁻¹ upon 18 O₂ substitution, as expected. This mode is shifted up by 4 cm⁻¹ as compared to this mode in WT *Pcc*GCS, which is likely associated with a non-hydrogen bonded O₂ form, indicating that the R78G mutation induced a significant conformational change which interrupted the H-bonding with heme-bound O₂. These data indicate that ligand-dependent heme propionate movement could induce larger

conformational changes in the heme active site, which is propagated to the signaling domain through the linker region, thereby impacting the catalytic efficiency and behavior of the enzyme. These results also support a role for R78 in sensing $\rm O_2$ binding through the heme propionates and support the enzyme kinetics data that suggest that hydrogen bonding between R78 and heme propionate is necessary for ligand-dependent DGC activity.

3.4. Conformational analysis of PccGCS WT and variants

As full-length PccGCS WT and variants have been recalcitrant to structural characterization by both crystallization and cryo-electron microscopy, small angle X-ray scattering (SAXS) and analytical ultracentrifugation (AUC) were used to provide information on protein conformation. SAXS uses the high-resolution structural models of individual domains to build homology models and combine them into a tertiary structure by fitting into the solvent envelope using rigid-body modelling tools. This approach has been applied to model the PccGCS tetramer using individual structures of diguanylate cyclase and globin domains well established with numerous examples in the protein database (rcsb.org). The radius of gyration and maximum diameter as from the Guinear analysis as well as the distance distribution function for the PccGCS WT and variants agree with values obtained for a tetramer in the case of PccGCS WT, W86H and R78G variants and a dimer in H237A/ K238A variant (Table S2, Fig. S3). Fitting homology structures of the domain dimers (based on previously crystallized dimer structures from BpeGlobin [16] and EcDosC [13], the E. coli GCS) into the SAXS generated solution envelope results in a tightly assembled dimer of dimers (Fig. 5).

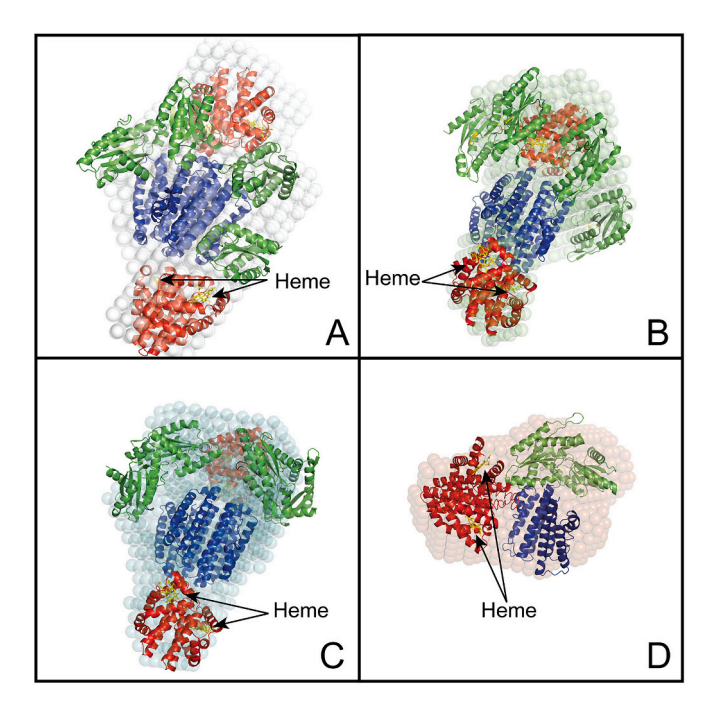


Fig. 5. SAXS models of selected variants: A) PccGCS WT, B) W86H, C) R78G, and D) H237A/K238A. Heme are shown in yellow and marked in one dimer within each panel. The cyclase domains are nucleotide-free and therefore GTP/c-di-GMP are not depicted in the models. Transparent spheres represent the particle reconstruction from DAMMIN/DAMMIF. Ribbon models represent the best fitting of domains to density ($\chi 2 \approx 1$). Domains are highlighted by colour as globin (red), middle (blue), and DGC (green). Heme cofactor is highlighted yellow. A, B, and C each represent tetrameric PccGCS and display similar overall architecture. D represents the dimeric form of PccGCS H237A/K238A, where the relative orientation of the three domains are different compared to that seen in the tetrameric state. (For interpretation of the references to colour in this figure legend, the reader is referred to the web version of this article.)

The overall structure of the PccGCS tetramer (Fig. 5A) forms a compact assembly and is held together by a bundle of previously identified π -helices formed by the middle domains of the four monomers and required for cyclase activity. The middle domains are modeled as a dimer of dimers, with monomers of each middle domain dimer modeled as parallel, based on the crystal structure of isolated middle domains from EcDosC, and the dimers modeled as antiparallel, which aligns the N-termini of the middle domains near the C-termini of their respective globin domains. The middle domain π -helix was previously been demonstrated to be involved in controlling cyclase activity [65] as the H237A/K238A variant exhibited >20-fold lower diguanylate cyclase activity. In addition, previous work identified crosslinks between the π -helix and globin domain and these results are further substantiated by the close interactions observed between these regions in the fitted SAXS models. In the PccGCS WT SAXS model, the sensor globin dimers are at each end of a tetrameric assembly of middle domains, with the cyclase domains making contacts with one face of the middle domain assembly. Given the flexible linkers between globin, middle, and cyclase domains and cross-linking data [65], it is likely that the cyclase domain can move relative to the globins, resulting in direct inter-domain contacts. In addition, the optimized model places cyclase domains within a dimer near each other, but each DGC dimer can be modeled in either the active (4URG [34]) or inactive (4URS [34]) conformations using crystal structures of active and inactive DGC domains, respectively. While the globin, middle, and cyclase dimers are expected to form between domains in the same two polypeptides, higher resolution structural data is necessary to observe the inter-domain linkers and definitively identify the connections. These results suggest that the cyclase domains are flexible, and that DGC domain orientation can be further optimized for greater cyclase activity, which is supported by data showing the PccGCS W86H variant exhibits ~3-fold greater cyclase activity than WT (Table 2). Frictional coefficient ratios (f/f_0) obtained by AUC identified differences between PccGCS WT in the Fe(II) and Fe(II)-O2 states (Fig. 6, S5, S6), further supporting roles for conformational flexibility and rearrangements in controlling DGC activity.

The SAXS envelope of the PccGCS W86H variant has a similar overall shape to that of PccGCS WT, but greater asymmetry along the globinmiddle-globin axis (Fig. 5C, S5). The larger frictional coefficient obtained by AUC, as compared to WT, suggests that PccGCS W86H is less spherical, also supporting the loss of symmetry (Fig. 6B). Modelling of the tetramer resulted in tighter assembly between the DGC domains, which is consistent with the Fe(II)-O₂ W86H variant having the highest cyclase activity of any PccGCS variants characterized to date. The model overall exhibits a more compact configuration, with the DGC domains interacting closely with the middle domain core. However, surprisingly, both DGC domain dimers are localized asymmetrically towards the same globin dimer (Fig. S7), instead of residing in a more centralized location. While there are sufficient residues in linking regions that are not included in the domain models to account for the migration, the mechanism that allows for the migration of the four diguanylate cyclase domains towards the same globin dimer is unknown and requires further investigation. The movement towards one globin dimer puts one product binding inhibitory site (I-site) of each DGC dimer within van der Waals contact with the globin (Fig. S8), which may facilitate cyclase domain positioning for optimal catalysis, as mutating the I-site (PccGCS R377A) previously was shown to substantially decrease diguanylate cyclase activity [23]. For PccGCS WT, the loop containing R78 of one sensor globin within a dimer is within ~ 10 Å of a diguanylate cyclase domain helix, suggesting that protein motions may allow interactions between DGC and a key heme-interacting residue. In addition, the heme pocket rearrangements and heme flattening observed in the rR spectra for PccGCS W86H may results in conformational changes within the globin domains that result in reorientation within the tetramer. PccGS W86H also exhibits significant changes in conformation due to O₂ binding, with the Fe(II) state resulting in two distinct frictional coefficients of similar concentration, one of which ($f/f_0 = 1.3$) is similar to

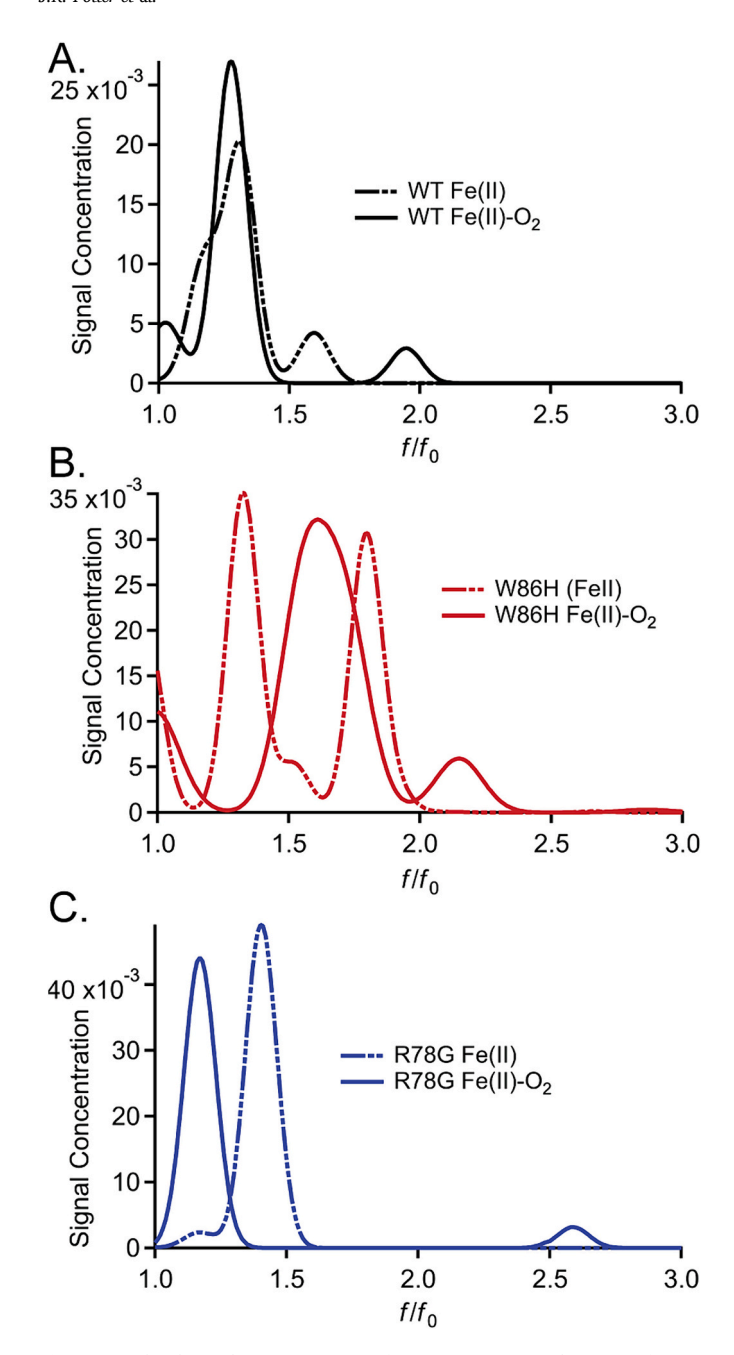


Fig. 6. O_2 binding alters PccGCS conformation. Frictional ratios of Fe(II) unligated and Fe(II)- O_2 states for PccGCS (A.) WT, (B.) W86H, and (C.) R78G obtained from AUC.

the conformation observed for WT while the second ($f/f_0 = 1.8$) corresponds to a less spherical, potentially elongated conformation (Fig. 6, S6).

The SAXS model of *Pcc*GCS R78G maintains an overall compact structure, similar to *Pcc*GCS WT and W86H, but blends conformational features (Fig. 5B). The cyclase domains are located near one globin dimer, highlighting a similar asymmetric shift to that observed for the W86H variant (Fig. 5, S7). However, the cyclase domains are farther apart than for W86H and are not well fit by the active dimer configuration, suggesting that the R78G variant does not result in fully activated cyclase domains. The frictional coefficients for both the Fe(II) unligated and Fe(II)-O₂ states are also more similar to *Pcc*GCS WT (Fig. 6), suggesting that the species observed for W86H with larger frictional coefficients correspond to conformations with higher catalytic activity.

Based on similarity to the *B. pertussis* globin and the resonance Raman spectra, the *Pcc*GCS R78 residue hydrogen bonds with a heme propionate and mutation of this position results in altered propionate conformation. These data suggest that the R78-propionate hydrogen bond is required for both differentiating between Fe(II)-unligated/Fe(II)-O₂ bound states of the heme and maintaining a more symmetrical domain arrangement. In addition, some tilting of the globin dimer towards the DGC/Middle domain interface is observed, providing further evidence supporting direct globin dimer interactions in DGC activity modulation. However, the change in relative position of the DGC domains is not sufficient to yield maximal DGC activity, as observed in the W86H variant. The blending of WT and W86H features is supported by the rR spectra, as the R78G variant exhibits less heme ruffling but more vinyl out of plane bending, suggesting that overall heme flattening is required for maximal DGC activation.

In contrast to tetrameric assemblies of *PccGCS* WT and heme pocket variants, mutation of a π -helix within the middle domain results in primarily dimeric protein and nearly inactive enzyme [65]. SAXS analysis of the π -helix variant results in a compact dimer, with the globin and DGC domain dimers in proximity on one end of the middle domain dimer, although missing interactions at the I-site (Fig. 5D). The orientations of the globin and DGC dimers relative to the middle domains in the π -helix variant are altered, as compared to PccGCS WT, possibly because the contacts found within tetrameric GCS assemblies are required for positioning of the DGC domains in an "on" conformation. Taken together, the SAXS studies suggest a model for activation in which O₂ binding to the sensor globin domain results in rearrangements, potentially through direct interdomain contacts, that result in repositioning of the DGC domains to bring the active sites together for catalysis (Fig. 7). In contrast, mutation of the signal transducing π -helix eliminates cyclase activation and decreases basal activity by disrupting the tetramer interface in the middle domain and increasing the distance between DGC domain active sites. The close contacts between domains in the compact tetramers therefore allows for subtle changes in the heme pocket that occur upon ligand binding to be translated into relative orientations of DGC domains, controlling cyclase activity.

Our studies have demonstrated that heme edge residues play key roles in controlling both O2 affinity and cyclase activation in DGC-GCS proteins. Furthermore, we have used resonance Raman spectroscopy to determine that a heme edge aromatic residue (W86) modulates cyclase activity by controlling heme distortion and conformation. Using SAXS, we have shown that mutations that increase diguarylate cyclase activity result in asymmetrical positioning of the DGC domains active sites in close proximity. Mutation of propionate hydrogen-bonding residue (R78) results in O2-insensitive enzyme through changes to heme conformation and elimination of hydrogen bonding to the bound O2. In addition, the SAXS data yielded novel structural information on a fulllength tetrameric GCS protein, providing insights into inter-domain and inter-monomer interactions within a tetrameric GCS. This work suggests that heme conformation and hydrogen bonding can be transmitted through globin conformational changes to modulate GCS assembly symmetry and DGC activity. While high resolution structures are still needed, these studies highlight important residues in the globin and middle domains that alter protein conformation and modulate DGC activity, which could affect c-di-GMP related phenotypes, such as biofilm formation.

CRediT authorship contribution statement

Jacob R. Potter: Writing – original draft, Methodology, Investigation, Conceptualization. Shannon Rivera: Writing – original draft, Methodology, Investigation, Conceptualization. Paul G. Young: Writing – original draft, Methodology, Investigation, Conceptualization. Dayna G. Patterson: Methodology, Investigation. Kevin E. Namitz: Methodology, Investigation. Neela Yennawar: Writing – review & editing, Writing – original draft, Methodology, Investigation. James R. Kincaid:

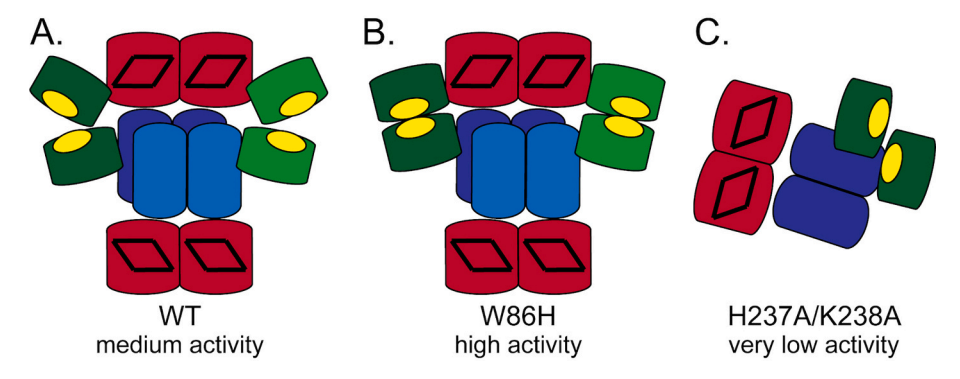


Fig. 7. Diguanylate cyclase activity is controlled by changing relative orientation of DGC (green) active sites (yellow ovals). PccGCS WT (A.) positions the active sites within each dimer in a close but suboptimal orientation, while W86H (B.) aligns the active sites at the end of the middle domains (blue) near one globin dimer (red). The π -helix variant results in formation of a dimer with DGC active sites held apart. (For interpretation of the references to colour in this figure legend, the reader is referred to the web version of this article.)

Writing – original draft, Supervision, Project administration, Methodology, Investigation, Funding acquisition, Conceptualization. Yilin Liu: Writing – review & editing, Writing – original draft, Project administration, Methodology, Investigation, Funding acquisition, Formal analysis, Conceptualization. Emily E. Weinert: Writing – review & editing, Writing – original draft, Supervision, Project administration, Methodology, Investigation, Formal analysis, Conceptualization.

Declaration of competing interest

The authors declare the following financial interests/personal relationships which may be considered as potential competing interests.

Emily Weinert reports financial support was provided by National Science Foundation. Emily Weinert reports financial support was provided by Herman Frasch Foundation for Chemical Research. Yilin Liu reports financial support was provided by National Science Foundation. If there are other authors, they declare that they have no known competing financial interests or personal relationships that could have appeared to influence the work reported in this paper.

Data availability

Data will be made available on request.

Acknowledgements

These studies are dedicated in memory of Professor Jim Kincaid, who was a wonderful scientist, mentor, and friend. This work was supported by NSF CHE1352040 (E.E.W.), NSF CHE2003350 (E.E.W.), NSF CHE2312149 (E.E.W. and Y.L.) and Frasch Foundation Grant 824-H17 (E.E.W.). We thank members of the Weinert lab for assistance and helpful suggestions. This work is based upon research conducted at the CHESS, which is supported by the NSF & NIH/NIGMS via NSF award DMR-1829070, and the MacCHESS resource is supported by NIH/ NIGMS award GM-124166. We sincerely appreciate the generous assistance from Drs. Qing Qiu Huang and Richard Gillilan at CHESS. Data collection at Penn State was supported by SIG S10 of the National Institutes of Health under award number S10-OD028589 for the smallangle X-ray scattering, S10-OD032215 for the Optima AUC, and S10 OD030490 for the Wyatt SEC-MALS-DLS system to NHY. The authors also thank Julia Fecko at the Huck X-ray Crystallography core for assistance in collecting the SEC-MALS and AUC data.

Appendix A. Supplementary data

Supplementary data to this article can be found online at https://doi.org/10.1016/j.jinorgbio.2024.112638.

References

- J. Green, M.D. Rolfe, L.J. Smith, Transcriptional regulation of bacterial virulence gene expression by molecular oxygen and nitric oxide, Virulence 5 (2014) 794–809
- [2] J.L. Burns, D. Douglas Deer, E.E. Weinert, Oligomeric state affects oxygen dissociation and diguanylate cyclase activity of globin coupled sensors, Mol. BioSyst. 10 (2014) 2823–2826.
- [3] C. Wu, Y.Y. Cheng, H. Yin, X.N. Song, W.W. Li, X.X. Zhou, L.P. Zhao, L.J. Tian, J. C. Han, H.Q. Yu, Oxygen promotes biofilm formation of Shewanella putrefaciens CN32 through a diguanylate cyclase and an adhesin, Sci. Rep. 3 (2013) 1945–1951.
- [4] H. Sawai, S. Yoshioka, T. Uchida, M. Hyodo, Y. Hayakawa, K. Ishimori, S. Aono, Molecular oxygen regulates the enzymatic activity of a heme-containing diguanylate cyclase (HemDGC) for the synthesis of cyclic di-GMP, Biochim. Biophys. Acta 1804 (2010) 166–172.
- [5] T. Shimizu, D. Huang, F. Yan, M. Stranava, M. Bartosova, V. Fojtíková, M. Martínková, Gaseous O2, NO, and CO in signal transduction: structure and function relationships of Heme-based gas sensors and Heme-redox sensors, Chem. Rev. 115 (2015) 6491–6533.
- [6] S.N. Vinogradov, M. Tinajero-Trejo, R.K. Poole, D. Hoogewijs, Bacterial and archaeal globins - A revised perspective, Biochim. Biophys. Acta 1834 (2013) 1789–1800.
- [7] J.A. Walker, S. Rivera, E.E. Weinert, Mechanism and role of globin coupled sensor signaling, Adv. Microb. Physiol. 71 (2017) 133–169.
- [8] U. Romling, M.Y. Galperin, M. Gomelsky, Cyclic di-GMP: the first 25 years of a universal bacterial second messenger, Microbiol. Mol. Biol. Rev. 77 (2013) 1–52.
- [9] J.L. Burns, P.B. Jariwala, S. Rivera, B.M. Fontaine, L. Briggs, E.E. Weinert, Oxygen-dependent globin coupled sensor signaling modulates motility and virulence of the plant pathogen Pectobacterium carotovorum, ACS Chem. Biol. 12 (2017) 2070–2077
- [10] R. Hengge, Principles of c-di-GMP signalling in bacteria, Nat. Rev. Microbiol. 7 (2009) 263–273.
- [11] X. Wan, J.R. Tuckerman, J.A. Saito, T.A. Freitas, J.S. Newhouse, J.R. Denery, M. Y. Galperin, G. Gonzalez, M.A. Gilles-Gonzalez, M. Alam, Globins synthesize the second messenger bis-(3'-5')-cyclic diguanosine monophosphate in bacteria, J. Mol. Biol. 388 (2009) 262–270.
- [12] W. Zhang, G.N. Phillips Jr., Crystallization and X-ray diffraction analysis of the sensor domain of the HemAT aerotactic receptor, Acta Crystallogr. D Biol. Crystallogr. 59 (2003) 749–751.
- [13] M. Tarnawski, T.R. Barends, I. Schlichting, Structural analysis of an oxygenregulated diguanylate cyclase, Acta Crystallogr. D Biol. Crystallogr. 71 (2015) 2158–2177
- [14] M. Stranava, V. Martinek, P. Man, V. Fojtikova, D. Kavan, O. Vanek, T. Shimizu, M. Martinkova, Structural characterization of the heme-based oxygen sensor, AfGcHK, its interactions with the cognate response regulator, and their combined mechanism of action in a bacterial two-component signaling system, Proteins 84 (2016) 1375–1389.
- [15] M. Stranava, P. Man, T. Skalova, P. Kolenko, J. Blaha, V. Fojtikova, V. Martinek, J. Dohnalek, A. Lengalova, M. Rosulek, T. Shimizu, M. Martinkova, Coordination and redox state-dependent structural changes of the heme-based oxygen sensor AfGcHK associated with intraprotein signal transduction, J. Biol. Chem. 292 (2017) 20921–20935.
- [16] S. Rivera, P.G. Young, E.D. Hoffer, G.E. Vansuch, C.L. Metzler, C.M. Dunham, E. E. Weinert, Structural insights into oxygen-dependent signal transduction within globin coupled sensors, Inorg. Chem. 57 (2018) 14386–14395.
- [17] S. Rivera, J.L. Burns, G.E. Vansuch, B. Chica, E.E. Weinert, Globin domain interactions control heme pocket conformation and oligomerization of globin coupled sensors. J. Inorg. Biochem. 164 (2016) 70–76.
- [18] K. Kitanishi, K. Kobayashi, Y. Kawamura, I. Ishigami, T. Ogura, K. Nakajima, J. Igarashi, A. Tanaka, T. Shimizu, Important roles of Tyr43 at the putative heme distal side in the oxygen recognition and stability of the Fe(II)-O2 complex of

- YddV, a globin-coupled heme-based oxygen sensor diguanylate cyclase, Biochemistry 49 (2010) 10381–10393.
- [19] T. Ohta, H. Yoshimura, S. Yoshioka, S. Aono, T. Kitagawa, Oxygen-sensing mechanism of HemAT from Bacillus subtilis: a resonance Raman spectroscopic study, J. Am. Chem. Soc. 126 (2004) 15000–15001.
- [20] D.C. Patterson, Y. Liu, S. Das, N.H. Yennawar, J.P. Armache, J.R. Kincaid, E. E. Weinert, Heme-edge residues modulate signal transduction within a bifunctional Homo-dimeric sensor protein, Biochemistry 60 (2021) 3801–3812.
- [21] D.C. Patterson, M.P. Ruiz, H. Yoon, J.A. Walker, J.P. Armache, N.H. Yennawar, E. E. Weinert, Differential ligand-selective control of opposing enzymatic activities within a bifunctional c-di-GMP enzyme, Proc. Natl. Acad. Sci. USA 118 (2021).
- [22] W. Zhang, J.S. Olson, G.N. Phillips Jr., Biophysical and kinetic characterization of HemAT, an aerotaxis receptor from Bacillus subtilis, Biophys. J. 88 (2005) 2801–2814
- [23] J.L. Burns, S. Rivera, D.D. Deer, S.C. Joynt, D. Dvorak, E.E. Weinert, Oxygen and c-di-GMP binding control oligomerization state equilibria of Diguanylate cyclase-containing globin coupled sensors, Biochemistry 55 (2016) 6642–6651.
- [24] E.M. Boon, S.H. Huang, M.A. Marletta, A molecular basis for NO selectivity in soluble guanylate cyclase, Nat. Chem. Biol. 1 (2005) 53–59.
- [25] D.S. Karow, D. Pan, R. Tran, P. Pellicena, A. Presley, R.A. Mathies, M.A. Marletta, Spectroscopic characterization of the soluble guanylate cyclase-like heme domains from vibrio cholerae and Thermoanaerobacter tengcongensis, Biochemistry 43 (2004) 10203–10211.
- [26] E.E. Weinert, L. Plate, C.A. Whited, C. Olea Jr., M.A. Marletta, Determinants of ligand affinity and heme reactivity in H-NOX domains, Angew. Chem. Int. Ed. Eng. 49 (2010) 720–723.
- [27] J.B. Hopkins, R.E. Gillilan, S. Skou, BioXTAS RAW: improvements to a free open-source program for small-angle X-ray scattering data reduction and analysis, J. Appl. Crystallogr. 50 (2017) 1545–1553.
- [28] D. Franke, M.V. Petoukhov, P.V. Konarev, A. Panjkovich, A. Tuukkanen, H.D. T. Mertens, A.G. Kikhney, N.R. Hajizadeh, J.M. Franklin, C.M. Jeffries, D. I. Svergun, ATSAS 2.8: a comprehensive data analysis suite for small-angle scattering from macromolecular solutions, J. Appl. Crystallogr. 50 (2017) 1212–1225
- [29] D.I. Svergun, Determination of the regularization parameter in indirect-transform methods using perceptual criteria, J. Appl. Crystallogr. 25 (1992) 495–503.
- [30] D.I. Svergun, Restoring low resolution structure of biological macromolecules from solution scattering using simulated annealing, Biophys. J. 76 (1999) 2879–2886.
- [31] V.V. Volkov, D.I. Svergun, Uniqueness of ab initio shape determination in small-angle scattering, J. Appl. Crystallogr. 36 (2003) 860–864.
- [32] A. Waterhouse, M. Bertoni, S. Bienert, G. Studer, G. Tauriello, R. Gumienny, F. T. Heer, T.A.P. de Beer, C. Rempfer, L. Bordoli, R. Lepore, T. Schwede, SWISS-MODEL: homology modelling of protein structures and complexes, Nucleic Acids Res. 46 (2018) W296–W303.
- [33] The PyMOL Molecular Graphics System, Version 1.2r3pre, Schrödinger, LLC, 2024.
- [34] A. Deepthi, C.W. Liew, Z.-X. Liang, K. Swaminathan, J. Lescar, Structure of a Diguanylate cyclase from Thermotoga maritima: insights into activation, feedback inhibition and Thermostability, PLoS One 9 (2014) e110912.
- [35] F. Germani, M. Nardini, A. De Schutter, B. Cuypers, H. Berghmans, M.L. Van Hauwaert, S. Bruno, A. Mozzarelli, L. Moens, S. Van Doorslaer, M. Bolognesi, A. Pesce, S. Dewilde, Structural and functional characterization of the globincoupled sensors of Azotobacter vinelandii and Bordetella pertussis, Antioxid. Redox Signal. 32 (2020) 378–395.
- [36] E.F. Pettersen, T.D. Goddard, C.C. Huang, G.S. Couch, D.M. Greenblatt, E.C. Meng, T.E. Ferrin, UCSF Chimera-A visualization system for exploratory research and analysis, J. Comput. Chem. 25 (2004) 1605–1612.
- [37] A. Panjkovich, D.I. Svergun, Deciphering conformational transitions of proteins by small angle X-ray scattering and normal mode analysis, Phys. Chem. Chem. Phys. 18 (2016) 5707–5719.
- [38] J.L. Burns, D.D. Deer, E.E. Weinert, Oligomeric state affects oxygen dissociation and diguanylate cyclase activity of globin coupled sensors, Mol. BioSyst. 10 (2014) 2823–2826.
- [39] W. Zhang, G.N. Phillips, Structure of the oxygen sensor in Bacillus subtilis: signal transduction of chemotaxis by control of symmetry, Structure 11 (2003) 1097–1110.
- [40] A.L. Tsai, V. Berka, E. Martin, J.S. Olson, A "sliding scale rule" for selectivity among NO, CO, and O(2) by heme protein sensors, Biochemistry 51 (2012) 172–186
- [41] N.J. Hoque, S. Rivera, P.G. Young, E.E. Weinert, Y. Liu, Heme pocket hydrogen bonding residue interactions within the pectobacterium diguanylate cyclasecontaining globin coupled sensor: a resonance raman study, J. Inorg. Biochem. (2024) (Revised manuscript under review.).

- [42] T.G. Spiro, A.V. Soldatova, G. Balakrishnan, CO, NO and O2 as vibrational probes of Heme protein interactions, Coord. Chem. Rev. 257 (2013) 511–527.
- [43] S. Aono, T. Kato, M. Matsuki, H. Nakajima, T. Ohta, T. Uchida, T. Kitagawa, Resonance Raman and ligand binding studies of the oxygen-sensing signal transducer protein HemAT from Bacillus subtilis, J. Biol. Chem. 277 (2002) 13528–13538.
- [44] H. Yoshimura, S. Yoshioka, K. Kobayashi, T. Ohta, T. Uchida, M. Kubo, T. Kitagawa, S. Aono, Specific hydrogen-bonding networks responsible for selective O2 sensing of the oxygen sensor protein HemAT from Bacillus subtilis, Biochemistry 45 (2006) 8301–8307.
- [45] Y.L. Liu, J.R. Kincaid, Resonance Raman studies of gas sensing heme proteins, J. Raman Spectrosc. 52 (2021) 2516–2535.
- [46] W.A. Kalsbeck, A. Ghosh, R.K. Pandey, K.M. Smith, D.F. Bocian, Determinants of the vinyl stretching frequency in Protoporphyrins - implications for cofactorprotein interactions in Heme-proteins, J. Am. Chem. Soc. 117 (1995) 10959–10968.
- [47] M.P. Marzocchi, G. Smulevich, Relationship between heme vinyl conformation and the protein matrix in peroxidases, J. Raman Spectrosc. 34 (2003) 725–736.
- [48] Q. Huang, R. Schweitzer-Stenner, Non-planar heme deformations and excited state displacements in horseradish peroxidase detected by Raman spectroscopy at Soret excitation, J. Raman Spectrosc. 36 (2005) 363–375.
- [49] Z. Chen, T.W.B. Ost, J.P.M. Schelvis, Phe393 mutants of cytochrome P450 BM3 with modified Heme redox potentials have altered Heme vinyl and propionate conformations, Biochemistry 43 (2004) 1798–1808.
- [50] J.F. Cerda-Colón, E. Silfa, J. López-Garriga, Unusual rocking freedom of the Heme in the hydrogen sulfide-binding hemoglobin from <i>Lucina</i> <i>pectinata</i> i>, J. Am. Chem. Soc. 120 (1998) 9312–9317.
- [51] E.S. Peterson, J.M. Friedman, E.Y.T. Chien, S.G. Sligar, Functional implications of the proximal hydrogen-bonding network in myoglobin: A resonance Raman and kinetic study of Leu89, Ser92, His97, and F-Helix swap mutants [†], Biochemistry 37 (1998) 12301–12319.
- [52] K.B. Lee, E. Jun, G.N. La Mar, I.N. Rezzano, R.K. Pandey, K.M. Smith, F.A. Walker, D.H. Buttlaire, Influence of heme vinyl- and carboxylate-protein contacts on structure and redox properties of bovine cytochrome b5, J. Am. Chem. Soc. 113 (1991) 3576–3583.
- [53] F. Rwere, P.J. Mak, J.R. Kincaid, Resonance Raman interrogation of the consequences of Heme rotational disorder in myoglobin and its ligated derivatives, Biochemistry 47 (2008) 12869–12877.
- [54] T. Kitagawa, K. Nagai, M. Tsubaki, Assignment of the Fe-Nepsilon (his F8) stretching band in the resonance Raman-spectra of deoxy myoglobin, FEBS Lett. 104 (1979) 376–378.
- [55] D.L. Rousseau, J.M. Friedman, Transient and cryogenic studies of photodissociated hemoglobin and myoglobin, in: Biological Applications of Raman Spectroscopy (Spiro, T. G., Ed.), 1988, pp. 133–215.
- [56] J. Teraoka, T. Kitagawa, Structural implication of the Heme-linked ionization of horseradish-peroxidase probed by the Fe-histidine stretching Raman line, J. Biol. Chem. 256 (1981) 3969–3977.
- [57] G. Smulevich, M.A. Miller, J. Kraut, T.G. Spiro, Conformational change and histidine control of Heme chemistry in cytochrome-C peroxidase - resonance Raman evidence from Leu-52 and Gly-181 mutants of cytochrome-C peroxidase, Biochemistry 30 (1991) 9546–9558.
- [58] S. Dasgupta, D.L. Rousseau, H. Anni, T. Yonetani, Structural characterization of cytochrome-C peroxidase by resonance Raman-scattering, J. Biol. Chem. 264 (1989) 654–662.
- [59] A.V. Soldatova, T.G. Spiro, Alternative modes of O-2 activation in P450 and NOS enzymes are clarified by DFT modeling and resonance Raman spectroscopy, J. Inorg. Biochem. 207 (2020).
- [60] Y. Liu, I.G. Denisov, S.G. Sligar, J.R. Kincaid, Substrate-specific allosteric effects on the enhancement of CYP17A1 Lyase efficiency by cytochrome b5, J. Am. Chem. Soc. 143 (2021) 3729–3733.
- [61] Y. Liu, Y. Grinkova, M.C. Gregory, I.G. Denisov, J.R. Kincaid, S.G. Sligar, Mechanism of the clinically relevant E305G mutation in human P450 CYP17A1, Biochemistry 60 (2021) 3262–3271.
- [62] M. Gregory, P.J. Mak, S.G. Sligar, J.R. Kincaid, Differential hydrogen bonding in human CYP17 dictates hydroxylation versus Lyase chemistry, Angew. Chem. Int. Edit. 52 (2013) 5342–5345.
- [63] S. Muralidharan, E.M. Boon, Heme flattening is sufficient for signal transduction in the H-NOX family, J. Am. Chem. Soc. 134 (2012) 2044–2046.
- [64] C. Olea, E.M. Boon, P. Pellicena, J. Kuriyan, M.A. Marletta, Probing the function of Heme distortion in the H-NOX family, ACS Chem. Biol. 3 (2008) 703–710.
- [65] J.A. Walker, Y. Wu, J.R. Potter, E.E. Weinert, pi-Helix controls activity of oxygensensing diguanylate cyclases, Biosci. Rep. 40 (2020) BSR20193602.